remote sensing

MDPI

Article

A Training-Independent Sentinel-1/2 Phenological Approach for Interpretable Paddy Rice Mapping in Heilongjiang, China

Muhammad Nasar Ahmad [1], Lichuan Gu [1,*], Shuai Yang [1], Xiaohui Yuan [1,2] and George D. Bathrellos [3]

[1] School of Artificial Intelligence, Anhui Agricultural University, Hefei 230036, China; mnasarahmad@ahau.edu.cn (M.N.A.); yangs@ahau.edu.cn (S.Y.); xiaohui.yuan@unt.edu (X.Y.)
[2] Department of Computer Science and Engineering, University of North Texas, Denton, TX 76203, USA
[3] Department of Geology, University of Patras, Rio, 26504 Patras, Greece; gbathrellos@upatras.gr
* Correspondence: glc@ahau.edu.cn

Highlights

- A Sentinel-1/2 flood-to-green phenology framework effectively integrated optical and SAR evidence for 30 m paddy rice mapping.
- The training-independent, rule-based approach captured rice growth trajectories while maintaining transparent and interpretable classification decisions.
- - The framework provides a practical alternative to supervised training-dependent approaches for large-area rice monitoring.
- - The approach supports regional agricultural inventory and assessment in Heilongjiang and provides a basis for future application across other rice-growing regions.

Abstract

Accurate identification of paddy rice from satellite imagery is challenging in heterogeneous agricultural landscapes because water, wetland, and vigorous summer vegetation can exhibit spectral and radar responses similar to those of rice at individual observation dates. This study develops an interpretable, training-independent rice-mapping approach, meaning that the final classification does not rely on supervised classifier training, although manually interpreted locations were used for exploratory threshold selection. The approach identifies paddy fields from their characteristic transition from early-season inundation to subsequent canopy development. These phenological signals were integrated using explicit decision rules within a cropland-constrained domain, followed by persistent-water exclusion and spatial refinement. The framework was applied to the 2025 rice-growing season in the agricultural regions analyzed in Heilongjiang Province, China, using 30 m output mapping. Validation with 695 independent reference observations yielded an overall accuracy of 92.09%, Cohen's kappa of 0.791, rice producer's accuracy of 94.87%, user's accuracy of 75.90%, and an F1-score of 84.33%. The high producer's accuracy indicates effective detection of reference rice locations, whereas the lower user's accuracy shows that commission error remains the principal limitation, particularly in areas with moisture and vegetation conditions resembling paddy fields. Sequential screening further showed that combining phenological evidence with cropland and water constraints substantially reduced the candidate mapping domain. The proposed approach provides an auditable alternative to training-dependent classification workflows and offers a transparent basis for repeatable rice mapping and agricultural monitoring, while requiring further evaluation across multiple years and regions before broader operational transfer.

Academic Editors: Jinchang Ren, Jon Atli Benediktsson, Maher Assaad, Jaime Zabalza and Erlei Zhang

Received: 11 September 2026
Revised: 4 October 2026
Accepted: 12 October 2026
Published: 13 October 2026

Copyright: © 2026 by the author. Licensee MDPI, Basel, Switzerland. This article is an open access article distributed under the terms and conditions of the Creative Commons Attribution (CC BY) license.

Keywords: rice mapping; crop monitoring; Sentinel-1/2; SAR–optical data fusion; phenology-constrained classification; flood-to-green trajectory; agricultural remote sensing; precision agriculture

1. Introduction

Accurate, timely, and transferable rice mapping is essential for food-security assessment, agricultural management, irrigation planning, and crop production forecasting. Reliable information on rice distribution and dynamics supports regional agricultural monitoring and enables improved assessment of crop productivity under changing environmental conditions. However, existing rice mapping approaches are frequently developed for specific regions, rely on predefined processing workflows, or depend on single-season observations, limiting their transferability and operational application. Satellite remote sensing provides an effective solution by enabling repeated, spatially explicit, and large-area monitoring of agricultural systems. Recent advances in multi-source satellite observations, cloud computing, and geospatial analysis platforms have further improved the capability for operational crop monitoring from regional to national scales [1,2].

Rice cultivation exhibits a distinctive phenological trajectory that provides an important basis for satellite-based identification. Unlike many upland crops, paddy rice typically undergoes a characteristic transition from early-season flooding during field preparation and transplanting to rapid vegetation development during the growing season. During the flooding period, exposed water surfaces generate strong spectral responses in water-sensitive indices and characteristic radar backscatter variations, whereas later crop development produces increasing vegetation signals and modified microwave responses associated with canopy growth. Multi-temporal satellite observations have therefore been widely used to exploit the flood-to-green phenological trajectory for rice discrimination. Early studies demonstrated that integrating surface-water dynamics with vegetation development could effectively identify rice fields using satellite observations [3]. However, optical observations acquired during the short flooding period are often affected by cloud contamination, atmospheric interference, and confusion with other water-related surfaces, reducing the reliability of optical-only approaches [4].

The complementary characteristics of Sentinel-1 synthetic aperture radar (SAR) and Sentinel-2 multispectral imagery provide new opportunities to overcome these limitations. Sentinel-2 captures spectral variations associated with surface water, soil conditions, chlorophyll activity, and crop development, whereas Sentinel-1 provides frequent, weather-independent observations sensitive to surface roughness, inundation status, and vegetation structure through VV (Vertical–Vertical) and VH (Vertical–Horizontal) backscatter measurements [5]. The integration of SAR and optical observations enables a more complete characterization of rice phenological transitions than single-sensor approaches. In addition, cloud-based platforms such as Google Earth Engine (GEE) have substantially improved the feasibility of large-scale multi-temporal satellite processing by providing efficient access to satellite archives and scalable computational resources [6–8].

Recent research has substantially advanced rice mapping through multi-temporal satellite observations, machine-learning algorithms, automated sample generation, and phenology-based strategies. Earlier MODIS (Moderate Resolution Imaging Spectroradiometer) and Landsat studies established the feasibility of satellite-based rice monitoring and provided valuable information for historical agricultural analysis, while Sentinel missions improved spatial resolution and observation frequency. MODIS–Sentinel-1 fusion

approaches have combined temporal continuity with improved spatial detail for rice monitoring across heterogeneous landscapes [9], whereas Landsat-based investigations have supported long-term analysis of rice distribution changes across China [10,11].

The increasing availability of Sentinel-1 and Sentinel-2 time-series data has further promoted operational rice mapping by integrating complementary radar and optical information. Sentinel-1-based approaches have demonstrated advantages under persistent cloud conditions by maintaining observations throughout the rice-growing season [12]. To reduce dependence on manually collected training samples, automated mapping frameworks have recently been developed. For example, Ref. [13] proposed the Fully Automated Rice Mapping (FARM) framework, which integrated Sentinel-1 SAR and Sentinel-2 time-series imagery with automatic sample generation and machine-learning classification to support large-area rice mapping without extensive manual labelling. Similarly, Ref. [14] developed the Sentinel-1/-2 Phenology-enhanced paddy Rice (SPRC) framework, which combined Sentinel-2 phenological characteristics and Sentinel-1 temporal features with probabilistic Random Forest classification for automated rice mapping, including applications in Heilongjiang Province, China. These studies highlight the importance of integrating phenological information and multi-source satellite observations for improving rice mapping performance.

Despite these advances, several challenges remain for operational large-scale rice monitoring. Many high-performing approaches still depend on extensive reference samples, complex feature engineering, or machine-learning classifiers, which may reduce transferability across regions with different climates, planting calendars, and agricultural management practices. From an agricultural monitoring perspective, these limitations restrict the timely generation of reliable rice inventories required for crop statistics, production assessment, and regional agricultural planning. Although automated classification frameworks improve processing efficiency, their decision mechanisms often provide limited information regarding the physical evidence supporting individual classifications. Phenology-based methods improve interpretability by linking satellite observations with crop development processes; however, existing approaches frequently rely on fixed temporal windows, empirical thresholds, or regional calibration, which may reduce robustness under variable environmental conditions. Furthermore, most studies emphasize final classification accuracy while providing limited evaluation of intermediate evidence contributions, candidate-area reduction, and spatial uncertainty.

Unlike previous rice mapping approaches that rely primarily on supervised classification or isolated phenological indicators, this study develops an interpretable flood-to-green phenology framework that integrates complementary optical and radar evidence throughout the rice growth cycle. The proposed framework introduces transparent evidence-based decision rules, reduces dependence on extensive training samples, and provides explicit diagnostic uncertainty information, thereby supporting scalable, reproducible, and operational agricultural rice monitoring over large agricultural regions.

These limitations are particularly relevant in Heilongjiang Province, northeastern China, one of the world's largest high-latitude rice-producing regions. Rice cultivation in this region occurs within complex agricultural landscapes containing maize fields, soybean fields, wetlands, rivers, reservoirs, and other water-related surfaces. Previous studies have generated valuable rice products for northeastern China using Landsat, Sentinel observations, and machine-learning approaches; however, many existing products are either restricted to specific regions, developed for historical periods, or dependent on training datasets requiring periodic updating [15,16]. Therefore, a province-scale framework that directly integrates rice phenological characteristics with multi-source satellite observations while maintaining transparency, scalability, and diagnostic capability is still required.

To address this gap, this study develops a phenology-constrained Sentinel-1/2 flood-to-green framework for province-scale rice mapping in Heilongjiang Province, China. The framework integrates early-season Sentinel-2 water-sensitive indicators, Sentinel-1 VV/VH backscatter responses, vegetation development signals, cropland constraints, and permanent-water exclusion to identify rice fields according to their characteristic transition from inundation to canopy greening. Implemented in Google Earth Engine, the framework generates a 30 m rice distribution product using transparent evidence integration rather than dependence on black-box classification models. Independent reference samples are used to evaluate mapping accuracy, agreement statistics, omission and commission errors, and diagnostic uncertainty. In addition, the contributions of individual evidence components and sequential screening processes are quantified to improve understanding of the physical mechanisms underlying the classification. The objectives of this study are to:

(1) Develop an interpretable Sentinel-1/2 framework for large-scale rice mapping based on flood-to-green phenological evidence;
(2) Evaluate the complementary contributions of SAR and optical observations for identifying rice growth transitions;
(3) Quantify the effects of phenological constraints, land-cover masking, and spatial refinement on candidate reduction and classification uncertainty;
(4) Assess mapping performance and identify potential limitations for operational application.

2. Materials and Methods

Heilongjiang Province, located in northeastern China (Figure 1), is one of the country's major grain-producing regions and comprises 13 prefecture-level administrative divisions. Intensive rice cultivation is concentrated primarily in the Songnen and Sanjiang plains, whereas forests, uplands, wetlands, rivers, reservoirs, and extensive maize–soybean croplands characterize the broader provincial landscape. The province has a cold-temperate monsoon climate and is dominated by single-season rice cultivation, with spring flooding and transplanting followed by rapid canopy development during summer [17]. This seasonal transition produces a distinctive inundation-to-greening signal that can be detected using multi-temporal satellite observations [18,19].

The administrative boundary of Heilongjiang Province defined the spatial processing extent, whereas the effective classification domain was restricted by the cropland and water-exclusion masks used in the rice-mapping framework. Rice classification, however, was restricted to an analytical domain defined by the cropland mask, permanent-water and water-edge exclusions, and the availability of the satellite observations required by the phenological decision rules. Consequently, the processing extent should be distinguished from the effective classification domain. The frequent coexistence of rice paddies with wetlands and permanent or seasonally inundated water bodies presents substantial classification challenges, while the integration of radar-based inundation information with optical water and vegetation signals provides a physically interpretable basis for rice discrimination. The combination of extensive single-season rice cultivation, strong inundation-to-greening phenology, heterogeneous agricultural landscapes, and frequent coexistence of paddies with wetlands and permanent water makes Heilongjiang an appropriate region for evaluating an interpretable SAR–optical rice-mapping framework.



Figure 1. Location of the study area in Heilongjiang Province, China.

2.1. Data Sources

The rice-mapping workflow integrated Sentinel-1 synthetic aperture radar, Sentinel-2 multispectral imagery, ESA WorldCover, and the Joint Research Centre Global Surface Water dataset (Table 1). All image selection, temporal compositing, index calculation, logical classification, post-processing, and area estimation were implemented in Google Earth Engine (GEE; Google LLC, Mountain View, CA, USA), which supports cloud-based analysis of large Earth-observation archives [20].

Sentinel-2 surface-reflectance imagery was used to characterize early-season water conditions and subsequent canopy development. Sentinel-1 interferometric wide-swath observations containing VV and VH polarizations provided weather-independent information related to surface inundation and crop structure. The integration of these sensors was motivated by their complementary properties: optical observations characterize water and vegetation responses directly, whereas C-band SAR remains available under cloud cover and responds to changes in surface roughness, water conditions, and vegetation structure. Recent rice-mapping frameworks have similarly demonstrated the value of combining Sentinel-1 and Sentinel-2 observations across key phenological stages [21,22].

ESA WorldCover 2021 v200 was used to restrict the analysis to cropland. This product provides global land-cover information at 10 m resolution and was derived from Sentinel-1 and Sentinel-2 observations. Long-term water occurrence and seasonality from the JRC Global Surface Water dataset were used to remove persistent water bodies and reduce confusion with rivers, lakes, reservoirs, and wetlands [23,24].

Table 1. Datasets used in the rice-mapping framework.

Dataset	Principal Variables	Spatial Resolution	Function
Sentinel-2 surface reflectance	Blue, green, red, NIR and SWIR reflectance	10–20 m	Water, vegetation and canopy-development evidence
Sentinel-1 GRD	VV and VH backscatter	10 m	Radar-based early-season flood evidence

ESA WorldCover 2021 v200	Cropland class	10 m	Agricultural analysis mask
JRC Global Surface Water	Water occurrence and seasonality	30 m	Persistent-water removal and water-edge exclusion
Administrative boundaries	Province and prefecture boundaries	Vector	Clipping, mapping and area reporting
Reference observations	Rice and non-rice labels	Point	Independent accuracy assessment

2.2. Overview and Innovation of the Framework

This design (Figure 2) is particularly suitable for agricultural monitoring because it links satellite observations directly with crop establishment and growth processes rather than relying solely on statistical similarity. It first identifies early-season water or saturated-soil evidence, then requires the development of a vigorous summer canopy, and finally confirms the classification using either Sentinel-1 flood evidence or an optical increase in vegetation greenness. Cropland masking, permanent-water removal, and spatial cleaning are subsequently used to suppress environmentally implausible detections.

Recent automated frameworks have generated training samples from phenological signatures and subsequently applied Random Forest or ensemble classifiers. For example, FARM combines Sentinel-1-based sample generation with multiple Random Forest models, while SPRC incorporates Sentinel-1/2 phenology, feature selection, and probabilistic Random Forest voting. Rice-Sentinel adaptively identifies transplanting and rapid-growth phases from optical and radar time series, whereas other recent methods have developed sample-free phenological indices or object-based phenological features for large-area mapping.

In contrast, the present framework does not require supervised model training in its final implementation. Its principal innovation is an auditable decision architecture that:

(i) Links the classification directly to inundation-to-greening rice phenology.
(ii) Combines optical and SAR evidence through explicit Boolean rules.
(iii) Separates phenological evidence from environmental plausibility constraints.
(iv) Exports intermediate evidence layers for diagnostic assessment.
(v) Quantifies the progressive reduction of candidate areas. This design prioritizes interpretability and computational efficiency while retaining the complementary information supplied by optical and radar observations.

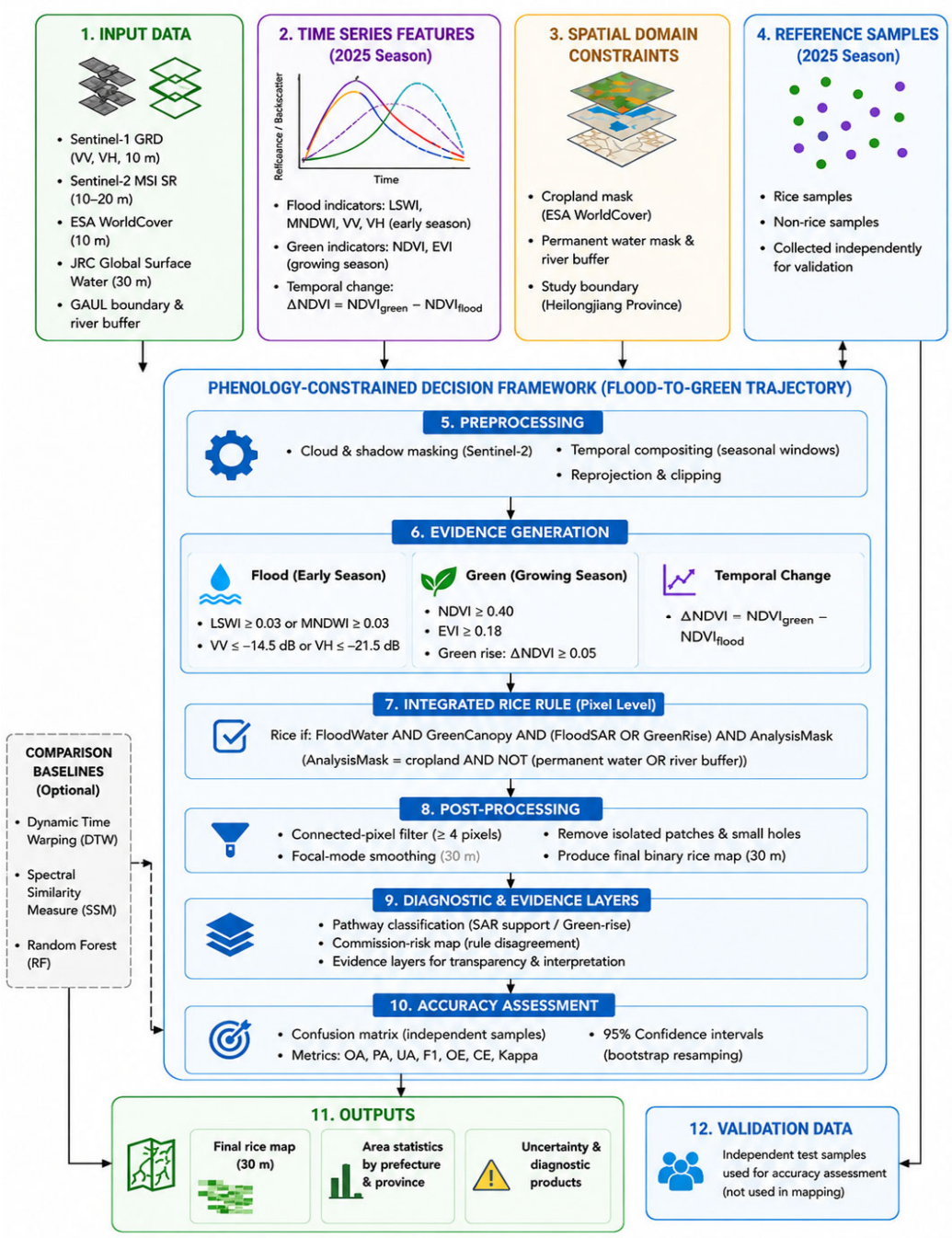


Figure 2. Conceptual workflow of the Sentinel-1/2 flood-to-green phenology framework for rice mapping in Heilongjiang Province. Sentinel-2 provides water, vegetation, and greenness-change indicators, while Sentinel-1 VV/VH backscatter offers complementary inundation evidence. The fused phenological signals are applied within a cropland-constrained domain after permanent-water and edge exclusion, followed by spatial filtering to generate the final 30 m rice map.

2.3. Image Pre-Processing and Seasonal Compositing

Two phenological periods were defined for the 2025 single-season rice cycle. The flooding and transplanting period extended from 1 May to 30 June, while the canopy-development period extended from 1 July to 31 August. These fixed windows were defined a priori to represent the expected phenological sequence of single-season paddy rice in Heilongjiang, from field inundation and transplanting in late spring to rapid canopy development during summer. The windows were selected to provide sufficiently broad temporal coverage for seasonal compositing rather than to identify exact planting dates

for individual fields. Their definition was guided by the regional rice-growing calendar and by the flood-to-green phenological behaviour reported in previous rice-mapping studies [25,26]. The temporal windows were specified before final classification and were not optimized using the independent validation samples.

Sentinel-2 observations were filtered spatially to Heilongjiang Province and temporally to the two phenological windows. Cloud-, cloud-shadow-, cirrus-, and snow-contaminated observations were excluded using the available Sentinel-2 quality information. Temporal percentile composites were then generated to reduce sensitivity to residual cloud contamination, isolated observations, and short-term spectral fluctuations. The 90th percentile of the water- and vegetation-sensitive indices was used to represent strong seasonal responses, while the median flood-season NDVI provided the early-season vegetation baseline.

Observation availability was quantified on a per-pixel basis after sensor-specific quality filtering. For Sentinel-2, valid observation counts were calculated separately for the May–June flooding/transplanting and July–August canopy-development periods after quality screening. For Sentinel-1, acquisition counts were calculated for the May–June flooding/transplanting period used to construct the SAR flood composite. Observation-count statistics were summarized within the effective analysis domain using the minimum, 25th percentile, median, 75th percentile, maximum, and proportion of pixels with zero valid observations.

Sentinel-1 Ground Range Detected (GRD) observations were obtained from the COPERNICUS/S1_GRD collection in Google Earth Engine and restricted to interferometric wide-swath (IW) acquisitions containing both VV and VH polarizations. The Google Earth Engine Sentinel-1 GRD collection is preprocessed using the ESA SNAP Sentinel-1 Toolbox (S1TBX v11.0.0), including thermal-noise removal, radiometric calibration, and terrain correction. No restriction was imposed on ascending or descending orbit direction; therefore, all qualifying IW VV/VH acquisitions intersecting the study domain were included. No additional incidence-angle normalization or explicit speckle filtering was applied. Flood-season VV and VH observations were summarized using the 10th percentile to emphasize the low-backscatter response associated with smooth or inundated surfaces.

Because C-band backscatter can vary with acquisition geometry, including incidence angle and orbit configuration, the adopted VV (−14.5 dB) and VH (−21.5 dB) flood-evidence thresholds were treated as empirical criteria for the 2025 seasonal composites rather than sensor-invariant physical thresholds. Their transfer to other regions, years, orbit configurations, or incidence-angle distributions may therefore require additional evaluation or regional recalibration. Similar temporal-feature and phenology-guided strategies have been adopted in recent regional and national rice-mapping studies [25,26].

2.4. Optical Indices and Phenological Evidence

Table 2 presents four spectral indices calculated from Sentinel-2 surface reflectance, including Normalized Difference Vegetation Index, Enhanced Vegetation Index, Land Surface Water Index, and Modified Normalized Difference Water Index. NDVI and EVI represented vegetation development, whereas LSWI and MNDWI characterized early-season water or saturated-surface conditions.

Table 2. Spectral indices used for identifying rice phenological characteristics in the flood-to-green mapping framework.

Indices	Formula	Purpose in Flood-to-Green Rice Mapping	Citation
Normalized Difference Vegetation Index (NDVI)	$NDVI = \frac{\rho_{NIR} - \rho_{Red}}{\rho_{NIR} + \rho_{Red}}$	Represents vegetation greenness and canopy development; NDVI increase indicates rice growth progression.	[27]
Enhanced Vegetation Index (EVI)	$EVI = \frac{2.5(\rho_{NIR} - \rho_{Red})}{\rho_{NIR} + 6\rho_{Red} - 7.5\rho_{Blue} + 1}$	Enhances vegetation sensitivity under dense canopy conditions by reducing soil and atmospheric effects.	[28]
Land Surface Water Index (LSWI)	$LSWI = \frac{\rho_{NIR} - \rho_{SWIR1}}{\rho_{NIR} + \rho_{SWIR1}}$	Detects surface moisture and flooding signals during rice transplanting stages.	[29]
Modified Normalized Difference Water Index (MNDWI)	$MNDWI = \frac{\rho_{Green} - \rho_{SWIR1}}{\rho_{Green} + \rho_{SWIR1}}$	Enhances open-water detection and reduces confusion with permanent water bodies.	[30]
Flood-to-green vegetation response (ΔNDVI **NDVI)**	$\Delta NDVI = NDVI_{green,p90} - NDVI_{flood,p50}$	Captures the flood-to-green phenological transition; higher values indicate stronger rice growth trajectories.	[3]

The use of water-sensitive indices during establishment and vegetation indices during subsequent growth follows the physical basis of phenology-based rice mapping. Recent methods have extended this principle through adaptive phenological phases, object-based features, automatic thresholds, and integrated optical–radar trajectories [17,31].

2.5. Evidence-Layer Construction

Early-season flood-water evidence was identified where either the flood-period LSWI or MNDWI exceeded its selected threshold. Green-canopy evidence required both high NDVI and high EVI during the summer canopy-development period. The optical green-rise condition required a positive increase in NDVI from the early flooding period to the summer vegetative period.

Sentinel-1 flood evidence was identified from low flood-season VV or VH backscatter. The OR relationship between the two polarizations allowed either channel to provide radar support, while the OR relationship between SAR flood evidence and optical green rise provides two alternative supporting pathways after the required optical flood-water and green-canopy conditions have been satisfied. It therefore increases flexibility in the supporting evidence but does not compensate for missing optical information required to establish flood-water or canopy evidence. Observation availability was evaluated separately from threshold response. A valid Sentinel-1 observation that did not satisfy the VV or VH flood threshold was treated as negative SAR evidence, whereas locations without valid observations were identified from the corresponding observation-count statistics. In the Boolean implementation, missing composite values were converted to zero after thresholding; therefore, the binary evidence layer itself does not distinguish threshold failure from missing observations.

Table 3 presents thresholds applied uniformly throughout the province.

Table 3. Final thresholds used in the framework.

Evidence Component	Final Criterion
Optical flood-water evidence	$LSWI_{flood,p90} > 0.03$ or $MNDWI_{flood,p90} > 0.03$
Green-canopy NDVI	$NDVI_{green,p90} > 0.40$
Green-canopy EVI	$EVI_{green,p90} > 0.18$
Optical green-rise response	$\Delta NDVI > 0.05$
Sentinel-1 VV flood evidence	$VV_{flood,p10} < -14.5\ dB$
Sentinel-1 VH flood evidence	$VH_{flood,p10} < -21.5\ dB$

Note: Sentinel-1 VV and VH thresholds are empirical values applied to the 2025 flood-season percentile composites and were not incidence-angle-normalized beyond the standard preprocessing of the GRD product.

The decision thresholds were selected through exploratory analysis of the seasonal index and backscatter distributions at manually interpreted rice and non-rice locations. Candidate values were examined for their ability to distinguish the expected flood-to-green response of rice from non-rice conditions while remaining consistent with the physical interpretation of the corresponding optical and SAR indicators and with previously reported rice phenology characteristics. The final thresholds were NDVI > 0.40 and EVI > 0.18 for green-canopy evidence, ΔNDVI > 0.05 for the optical green-rise response, LSWI > 0.03 or MNDWI > 0.03 for optical flood-water evidence, and VV < −14.5 dB or VH < −21.5 dB for SAR flood evidence. These values were fixed before the final accuracy assessment and were subsequently applied uniformly across the study domain without further optimization using the independent validation samples. They should therefore be interpreted as empirically selected regional decision criteria rather than universally applicable thresholds.

The exploratory threshold-selection set contained 100 rice and 100 non-rice locations distributed across representative agricultural and hydrologically influenced environments, including paddy fields, other cropland, and water-edge areas. These locations were separate from the 800 candidate locations used for independent accuracy assessment, with no shared points or fields.

The VV and VH thresholds were applied to the temporally composited, terrain-corrected backscatter data without explicit incidence-angle normalization. Because C-band backscatter varies with acquisition geometry, these thresholds should be regarded as study-specific empirical criteria, and their transfer to other regions, years, or orbit configurations may require additional evaluation or regional recalibration.

2.6. Analysis Mask and Rule-Based Classification

The analysis domain was restricted to World Cover cropland. Permanent water was defined using JRC Global Surface Water occurrence and seasonality thresholds, and the resulting water mask was expanded by a 60 m buffer to reduce confusion along water edges. Persistent surface water was removed using JRC water occurrence and seasonality information, and a buffer around the resulting water mask was excluded to reduce false detections along riverbanks, reservoir margins, and wetland edges. The final raw classification required the simultaneous presence of early flood-water evidence, summer canopy development, and at least one supporting flood-to-green pathway. To assess the influence of the ESA WorldCover 2021 cropland constraint on the 2025 classification, an additional sensitivity experiment was conducted in which the cropland restriction was removed while all other components of the framework were held unchanged. The permanent-water and water-edge exclusions, phenological thresholds, Sentinel-1/2 evidence rules, connected-component filtering, and neighbourhood-based spatial refinement were identical

to those of the baseline configuration. The unmasked classification was evaluated using the same independent validation samples as the WorldCover-constrained baseline. This phenology-based decision rule was expressed as Equation (1):

$$R_{raw} = F_{water} \cap G_{canopy} \cap (F_{SAR} \cup G_{rise}) \cap M_{analysis} \quad (1)$$

where F_{Water} denotes optical flood-water evidence, G_{canopy} denotes green-canopy evidence, F_{SAR} denotes radar flood evidence, G_{rise} denotes the flood-to-green NDVI increase, and $M_{analysis}$ denotes the final analysis mask.

Accordingly, the SAR/green-rise alternative operates only as a supporting condition; optical flood-water evidence and green-canopy evidence remain mandatory for every rice candidate. Unlike a conventional supervised classifier, this rule allows each mapped pixel to be traced directly to the biophysical evidence responsible for its inclusion. This transparency is particularly useful in landscapes where rice coexists with wetlands, water bodies, and other vigorous summer crops.

2.7. Spatial Post-Processing

The raw binary classification was refined using connected-component and neighbourhood operations (Equation (2)). Patches containing fewer than four connected rice pixels were removed to reduce isolated noise. A 30 m focal-mode operation was then used to fill small gaps and improve spatial coherence. The final post-processing operation can be written as:

$$R_{final} = FocalMode_{(30m)(R_{raw} \cap (ConnectedPixels \geq 4))} \quad (2)$$

where R_{final} represents the final rice distribution map after spatial refinement, $FocalMode_{30m}$ denotes a 30 m neighbourhood majority filter, R_{raw} is the initial rice candidate map, and $ConnectedPixels \geq 4$ removes isolated patches by retaining only connected components containing at least four pixels. The resulting provincial rice product was exported at 30 m resolution. Intermediate evidence layers were exported at 60 m to support diagnostic analysis and computationally efficient province-wide visualization.

To characterize the internal consistency of the supporting evidence, a rule-support layer was generated from the final mapped-rice pixels. Pixels satisfying both the Sentinel-1 flood condition and the optical green-rise condition were classified as strong-support rice, whereas mapped-rice pixels satisfying only one of these two supporting pathways were classified as reduced-support rice. Thus, strong support was defined as final rice AND SAR flood AND green rise, while reduced support was defined as final rice AND exactly one of SAR flood or green rise. This layer was used only to describe agreement between the two supporting pathways and was not interpreted as an independently validated error or uncertainty probability.

2.8. Sequential Screening and Area Calculation

The contribution of individual rules was evaluated by quantifying the proportion of candidate pixels retained after four sequential screening stages. These stages included (1) identification of flood-water evidence, (2) intersection of flood-water and green-canopy evidence, (3) restriction to the cropland-constrained analysis domain with supporting phenological conditions, and (4) final rice classification after spatial post-processing. The retention rate of each screening step was calculated using Equation (3), which measures the relative proportion of pixels maintained after each processing stage.

$$Retention\ rate = \frac{N_{current\ stage}}{N_{previous\ stage}} \times 100 \quad (3)$$

where $N_{\text{current stage}}$ represents the number of pixels retained after a specific screening operation, and $N_{\text{previous stage}}$ represents the number of pixels before applying that operation.

This metric quantifies the relative contribution of each rule independent of the total spatial extent.

Areas associated with the sequential screening stages were calculated using pixel-area weighting in Google Earth Engine rather than assuming a constant area from raster pixel counts. Rice area was calculated as:

$$A_R = \sum_{i=1}^{n} R_{ia_i} \quad (4)$$

where A_R represents the estimated rice area, R_i is the rice classification value of pixel i (1 for rice and 0 for non-rice), a_i represents the area of pixel i, and n denotes the total number of pixels within the analysis region. To ensure consistency among intermediate products with different native resolutions, all stage-area statistics were evaluated on a common 30 m equal-area grid (EPSG:6933). Binary evidence and classification masks were resampled using nearest-neighbour assignment, and pixel area was obtained using ee.Image.pixelArea(). Only valid pixels satisfying the corresponding stage mask were included in the area summation; masked and NoData pixels were excluded rather than treated as non-rice. Areas were initially calculated in square metres and subsequently converted to hectares by division by 10,000 and to million hectares (Mha) by division. The same processing boundary, target grid, and area-calculation settings were applied to all four screening stages to permit direct comparison. The final rice classification was maintained at 30 m resolution, whereas the 60 m diagnostic products were treated as separate outputs and were not used to derive the reported rice-area statistics. Component sensitivity was further evaluated by removing the Sentinel-1 flood pathway, optical green-rise pathway, cropland constraint, water-related exclusion, and focal-mode refinement individually, and by increasing the minimum connected-patch requirement from four to eight pixels. All other parameters were held constant, and each configuration was evaluated using the same reference samples.

2.9. Accuracy Assessment

A total of 800 candidate reference locations were evaluated for independent accuracy assessment. Candidate locations were manually interpreted using high-resolution imagery in Google Earth Pro (Google LLC, Mountain View, CA, USA; version 7.3.x) and assigned to rice or non-rice only when the reference class could be determined unambiguously. The reference imagery primarily covered 1 July to 31 August 2025, corresponding to the main canopy-development period of the 2025 rice-growing season. Locations with uncertain or mixed interpretation were excluded, removing 105 candidates and leaving 695 usable samples comprising 156 rice and 539 non-rice observations. Because exclusion was based on interpretability, difficult mixed or boundary conditions may be underrepresented in the final validation sample. The reference labels were used only for final accuracy assessment and were not used to optimize the classification thresholds. No explicit correction for spatial autocorrelation or local clustering was applied. The reported metrics therefore represent sample-based point accuracies rather than design-based area-adjusted estimates. Ninety-five-percent confidence intervals were estimated using a parametric multinomial bootstrap conditional on the observed 2 × 2 confusion matrix with 200,000 replicates; these intervals do not account for spatial clustering or map-area weighting. The validation results represent sample-based point accuracy rather than a design-based area-adjusted accuracy estimate. Because the available validation dataset did not include stratum inclusion probabilities or area weights, no area-weighted error matrix was calculated. In addition, no explicit correction for spatial autocorrelation or potential local clustering among reference locations was applied. Accordingly, the reported confidence intervals quantify uncertainty associated with the observed confusion matrix but should not be interpreted as accounting for spatial dependence in the validation sample. Overall accuracy,

rice producer's accuracy, rice user's accuracy, F1-score, omission error, commission error, and Cohen's kappa were calculated using Equation (5a–d). Ninety-five-percent confidence intervals were obtained by multinomial bootstrap resampling of the observed 2 × 2 confusion matrix. These intervals describe sampling uncertainty conditional on the observed class proportions and do not incorporate spatial-autocorrelation or area-weighting effects.

$$OA = \frac{TP+TN}{TP+TN+FP+FN} \quad (5a)$$

$$PA_{rice} = \frac{TP}{TP+FN} \quad (5b)$$

$$UA_{rice} = \frac{TP}{TP+FP} \quad (5c)$$

$$F1_{rice} = \frac{2(PA_{rice} \times UA_{rice})}{PA_{rice}+UA_{rice}} \quad (5d)$$

where TP, TN, FP, and FN denote true positive, true negative, false positive, and false negative pixels, respectively. OA represents overall classification accuracy, PA indicates the proportion of reference rice pixels correctly identified, UA measures the reliability of mapped rice pixels, and F1-score provides a balanced assessment of precision and recall.

Because the available assessment did not incorporate stratum inclusion probabilities or area weights, the reported values represent sample-based point accuracies rather than design-based, area-adjusted estimates. Probability sampling, area-weighted error matrices, and uncertainty intervals are recommended where unbiased class-area estimation is a primary objective [32].

3. Results

3.1. Provincial Rice Distribution and Mapped Area

Figure 3 shows the final classification delineated spatially coherent rice-growing areas within the analyzed agricultural regions of Heilongjiang Province. Mapped rice was concentrated primarily in low-lying and intensively cultivated landscapes where irrigation infrastructure and seasonal surface-water conditions support paddy-rice production. Comparatively fewer detections occurred in upland, forest-dominated, and non-agricultural areas.

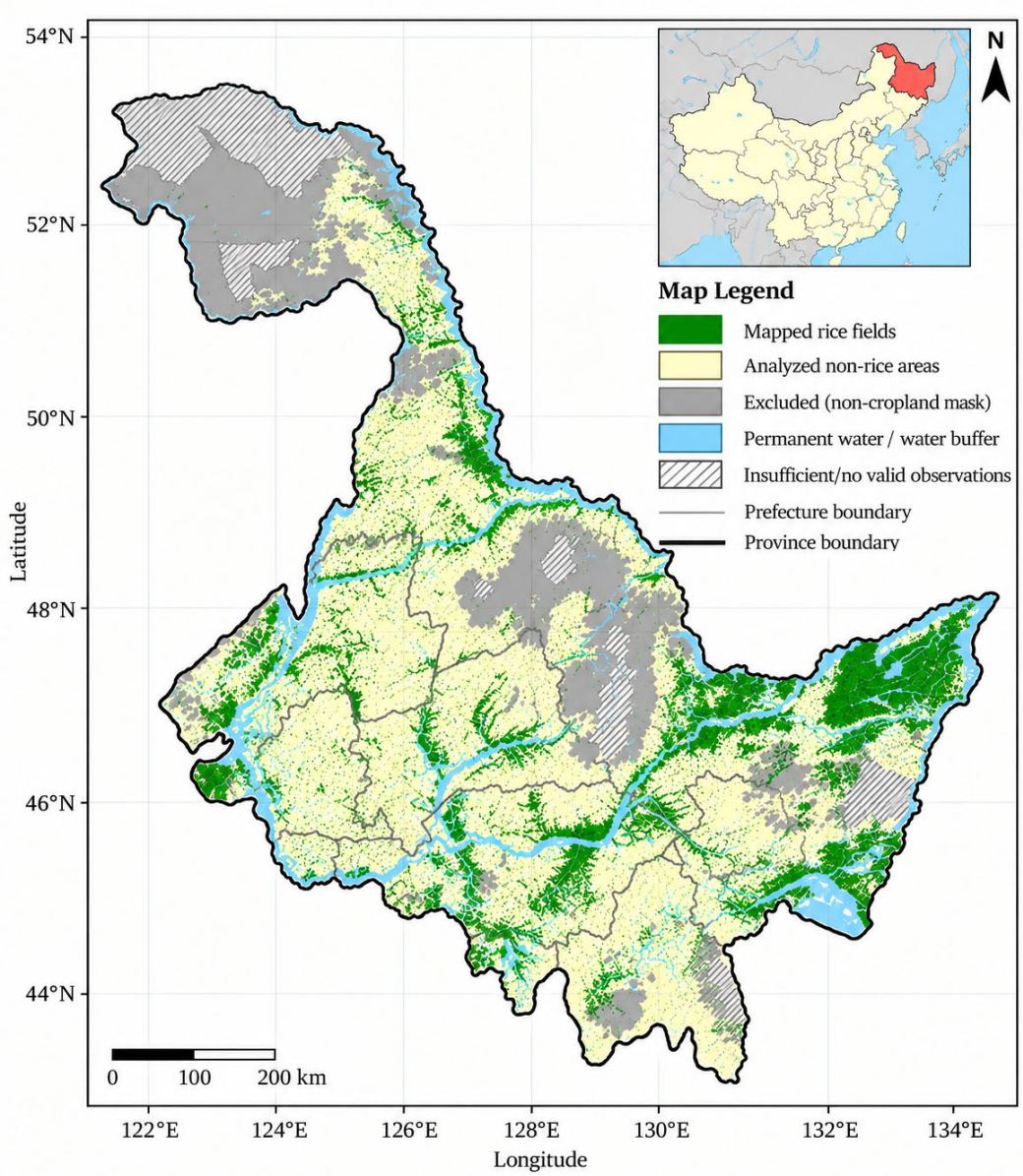


Figure 3. Spatial distribution of rice mapped using the Sentinel-1/2 flood-to-green phenology framework within the 2025 analysis domain in Heilongjiang Province, China. Green areas denote identified rice pixels, while administrative boundaries and geographic features provide spatial context. The displayed extent represents the effective analysis domain and should not be interpreted as complete provincial coverage.

The mapped distribution showed recognizable field-scale clustering and reflected the expected association between rice cultivation, flat terrain, and water availability. Representative field-scale patterns showed coherent alignment between mapped rice areas and individual agricultural parcels, supporting the spatial consistency of the final classification within the analyzed domain. Although satellite data were processed within the Heilongjiang provincial boundary, the effective rice-mapping domain was restricted by the cropland, water-exclusion, and valid-observation masks. Areas outside this domain were not eligible for classification and therefore should not be interpreted as confirmed non-rice.

Within the defined 2025 analysis domain, the final classification identified approximately 7.02 Mha of rice. This value was derived from the final binary rice raster using pixel-area weighting and therefore refers specifically to the effective classification domain

defined by the cropland, water-exclusion, phenological, and valid-data constraints applied in this study.

3.2. Spatial Characteristics of the Optical and Radar Evidence

Flood-water evidence occurred widely across agricultural areas and hydrologically influenced landscapes. This broad distribution showed that an early-season water signal alone was insufficient for reliable rice discrimination. Sentinel-1 flood evidence was more spatially restricted and provided independent support in areas exhibiting a low-backscatter flooding response.

Green-canopy evidence was also extensive because it included rice together with maize, soybean, and other vigorous summer vegetation. The final rice classification was substantially more constrained than any individual evidence layer because it required the logical intersection of flooding, canopy development, sensor support, and the analysis mask.

The evidence maps (Figure 4) therefore demonstrate that the framework did not treat water or vegetation as independently diagnostic of rice. Instead, rice was identified from the temporal and logical association of early inundation with subsequent canopy development.

Observation availability was generally sufficient across the effective analysis domain but varied spatially among sensors and phenological periods. During the May–June flooding/transplanting period, Sentinel-2 provided a median of 12 valid observations per pixel, with an interquartile range of 7–17 observations; 4.0% of pixels had no valid Sentinel-2 observation after quality screening. During the July–August canopy-development period, the median Sentinel-2 observation count was 13, with an interquartile range of 8–18 observations, and 3.0% of pixels had no valid observations. Sentinel-1 provided a median of seven May–June acquisitions per pixel, with an interquartile range of 4–10 observations, while only 0.5% of pixels had no valid SAR observation. These results indicate that the seasonal composites were supported by multiple observations over most of the analysis domain, although local gaps in optical availability remained because of cloud and quality screening.

For Sentinel-1, only 0.5% of pixels lacked a valid May–June observation, indicating that complete absence of SAR coverage was uncommon within the analysis domain. The straight or block-shaped patterns visible in the SAR flood-evidence layer therefore cannot be attributed solely to missing observations and may also reflect spatial variation in acquisition frequency or geometry together with percentile compositing and thresholding. Because these effects were not isolated individually, the origin of each boundary should be interpreted cautiously.

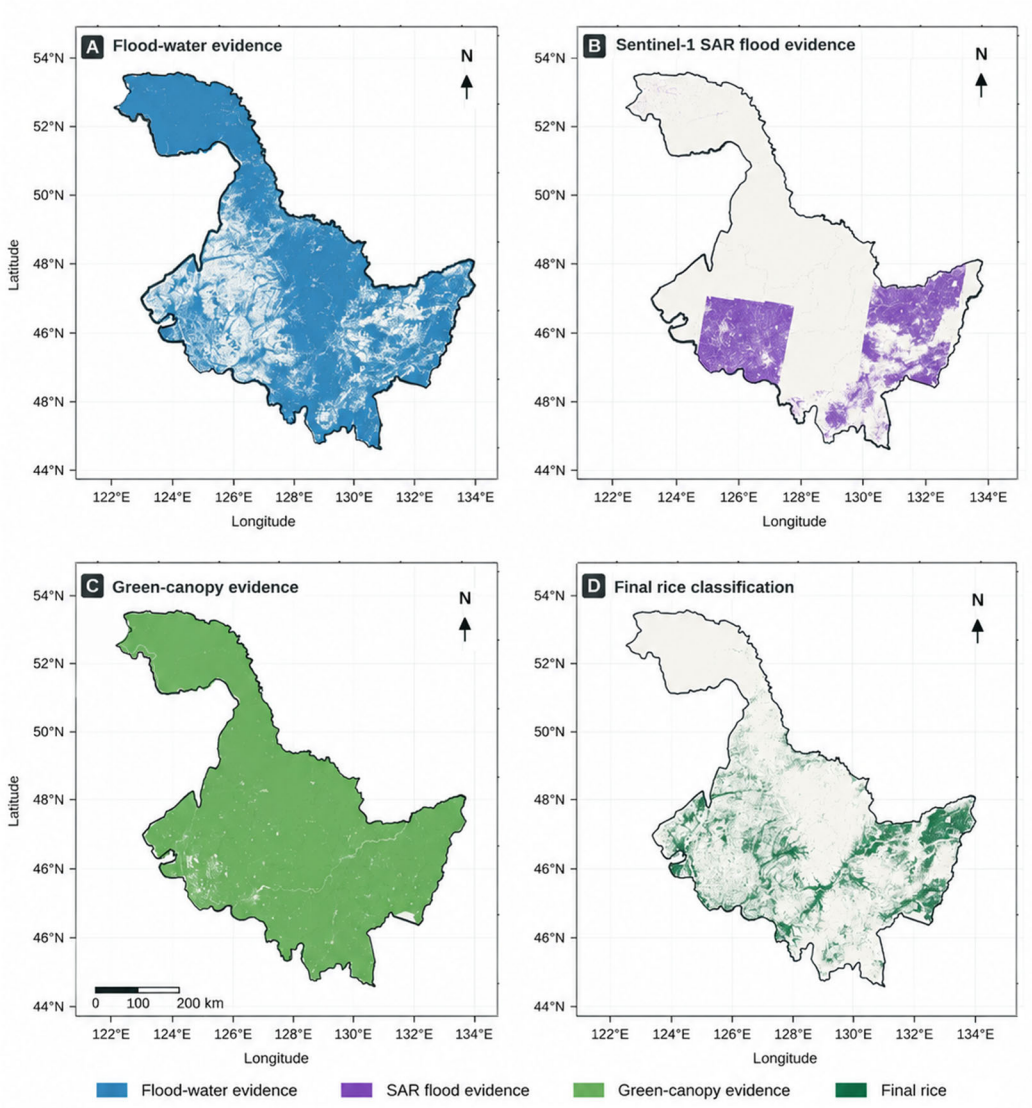


Figure 4. Spatial evidence layers used by the Sentinel-1/2 flood-to-green phenology framework for rice mapping in Heilongjiang Province in 2025. (**A**) Optical flood-water evidence during the field-flooding and transplanting period, (**B**) Sentinel-1 SAR flood evidence, (**C**) green-canopy evidence during the vegetative-growth period, and (**D**) the final rice classification. All panels use a common geographic extent and map scale to facilitate direct spatial comparison.

3.3. Rule-Based Classification Support

The rule-support layer distinguished mapped rice according to agreement between the two alternative supporting pathways. Rice pixels satisfying both SAR flood evidence and optical green-rise evidence were classified as strong-support pixels, whereas pixels satisfying only one of these pathways were classified as reduced-support pixels. Reduced-support pixels represented approximately 59.5% of the mapped rice area (Figure 5). This proportion quantifies pathway agreement within the rule-based framework and should not be interpreted as an error rate or probability of misclassification.

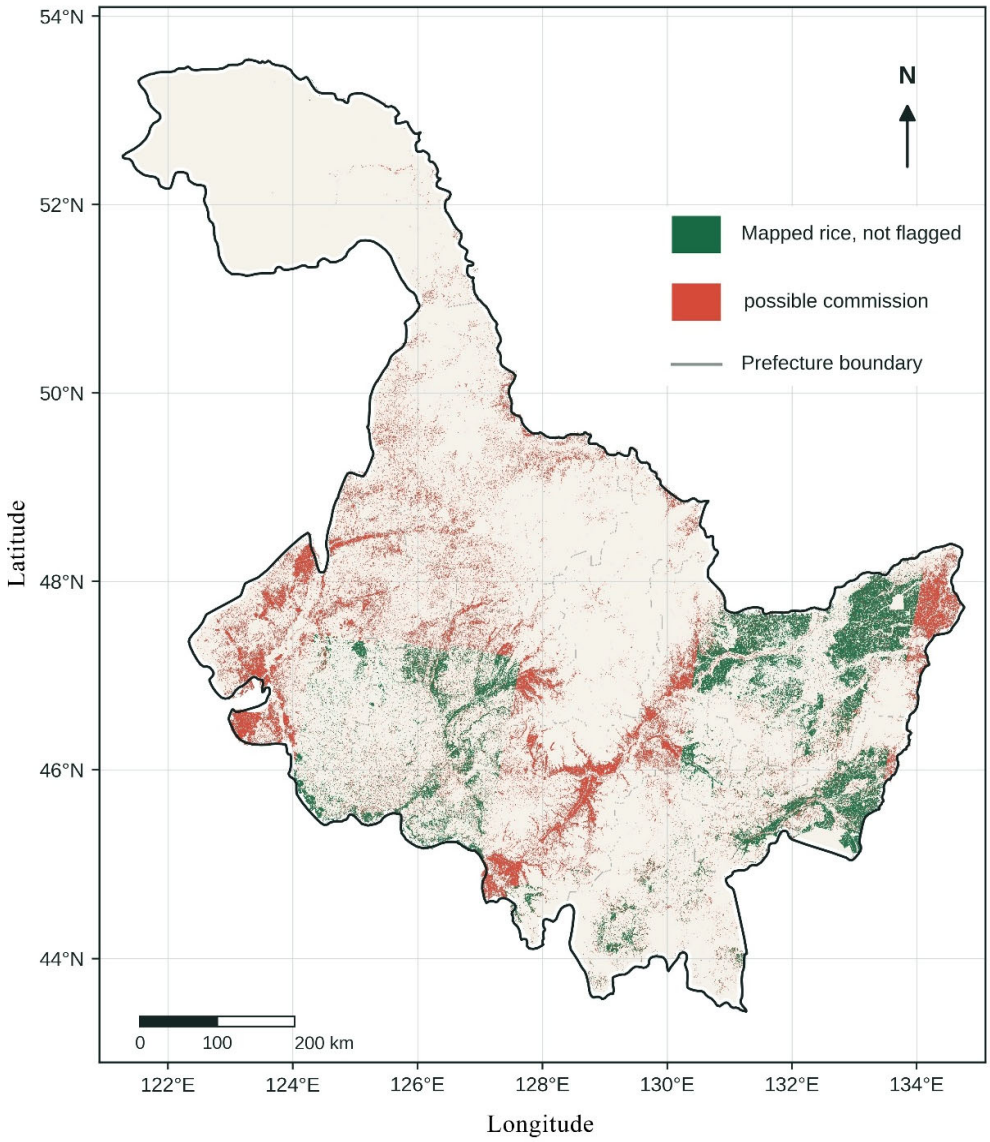


Figure 5. Rule-based classification-support map for the 2025 Heilongjiang rice classification. Dark green denotes mapped rice supported by both SAR flood and optical green-rise evidence, whereas red denotes reduced-support rice pixels supported by only one of these pathways. The support classes describe agreement between the two supporting pathways and do not represent probabilities of classification error.

3.4. Validation and Classification Accuracy

Figure 6 summarizes the validation-sample screening process. Of the 800 candidate validation locations, 105 were excluded because an unambiguous binary reference label could not be assigned, resulting in 695 usable samples (86.9% retention). The final validation set comprised 156 reference-rice samples and 539 reference non-rice samples. Among the 695 usable reference samples, 492 non-rice samples and 148 rice samples were correctly classified. Eight reference-rice samples were classified as non-rice, whereas 47 reference non-rice samples were classified as rice. The overall accuracy was 92.09%, and Cohen's kappa was 0.791. Rice producer's accuracy reached 94.87%, indicating that the framework detected most reference rice locations (Table 4). Rice user's accuracy was lower, at 75.90%, showing that commission error was the main limitation. The rice F1-score was 84.33%.

The rice omission error was 5.13%, whereas the commission error was 24.10%. Inspection of the 47 false-positive samples showed that 34 (72.3%) were other cropland with maize/soybean-type high-greenness responses, while five (10.6%) occurred near wetlands or water edges, five (10.6%) represented other vegetation or non-agricultural surfaces, and three (6.4%) were mixed or uncertain. The dominance of other cropland indicates that phenological similarity between rice and highly vegetated non-rice crops was the principal source of commission error. The results consequently indicate a classification with high rice sensitivity but more moderate reliability for locations labelled as rice. This pattern is consistent with residual confusion between rice and non-rice agricultural or wet surfaces satisfying similar early-water and summer-vegetation conditions.

Table 4. Accuracy metrics for the final rice map.

Metric	Value (95% CI)
Overall accuracy	92.09% (90.07–94.10%)
Cohen's kappa	0.791 (0.737–0.842)
Rice producer's accuracy	94.87% (91.16–98.05%)
Rice user's accuracy	75.90% (69.79–81.82%)
Rice F1-score	84.33% (80.00–88.22%)
Rice omission error	5.13% (1.95–8.84%)
Rice commission error	24.10% (18.18–30.21%)

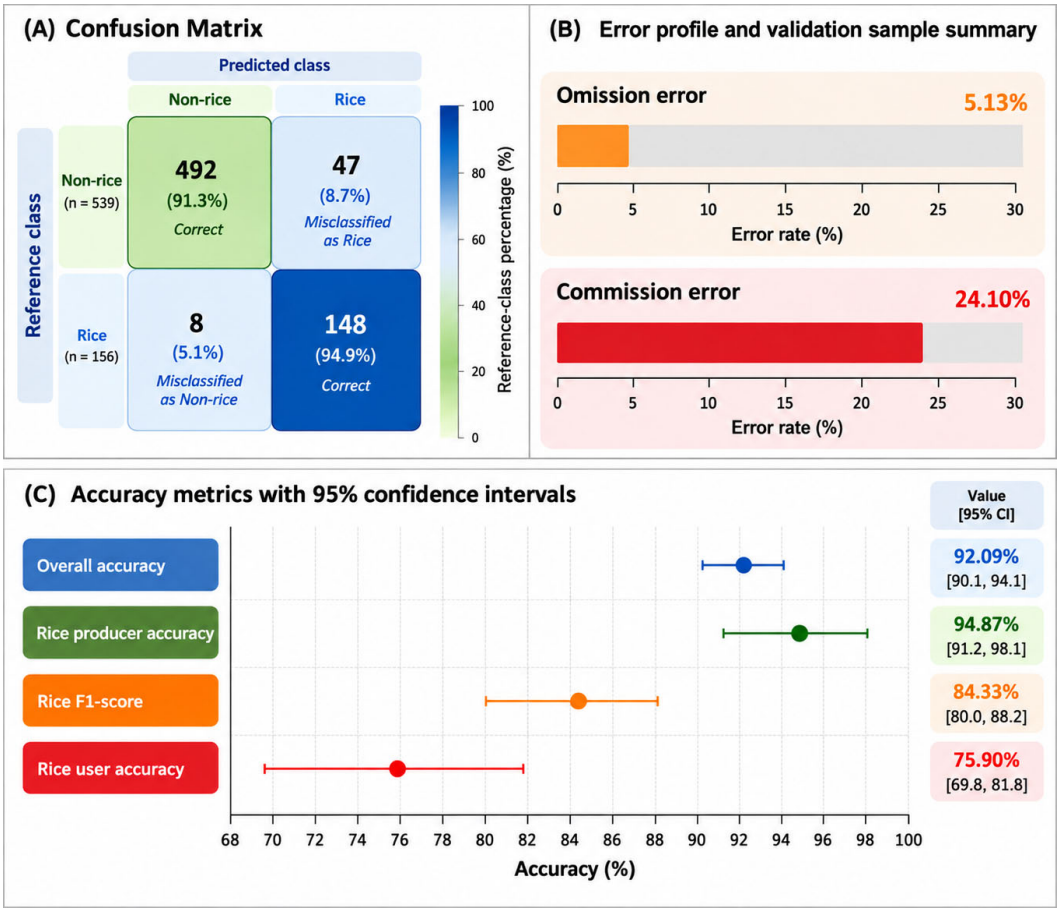


Figure 6. Validation and accuracy assessment of the 2025 Heilongjiang rice map using 695 usable reference samples. (**A**) Confusion matrix showing sample counts and row-normalized percentages, with reference classes presented as rows and mapped classes as columns. (**B**) Rice omission and commission errors together with the validation-sample summary. (**C**) Overall accuracy and rice-class producer's accuracy, user's accuracy, and F1-score with 95% confidence intervals.

3.5. Sequential Reduction of the Candidate Domain

The sequential screening analysis (Figure 7) demonstrated how the evidence layers progressively constrained potential rice locations within the study domain (Table 5). Early-season flood-water evidence generated the broadest candidate distribution. Its intersection with summer green-canopy evidence removed areas that exhibited water-related responses but lacked subsequent vegetation development.

Applying the cropland constraint and excluding permanent-water environments produced the largest spatial reduction, demonstrating the importance of environmental plausibility constraints for suppressing detections in rivers, reservoirs, wetlands, and non-agricultural surfaces. Sequential screening progressively reduced the spatial extent satisfying the rice-identification criteria. The final connected-component and neighbourhood filters further removed isolated pixels and small spatially inconsistent patches.

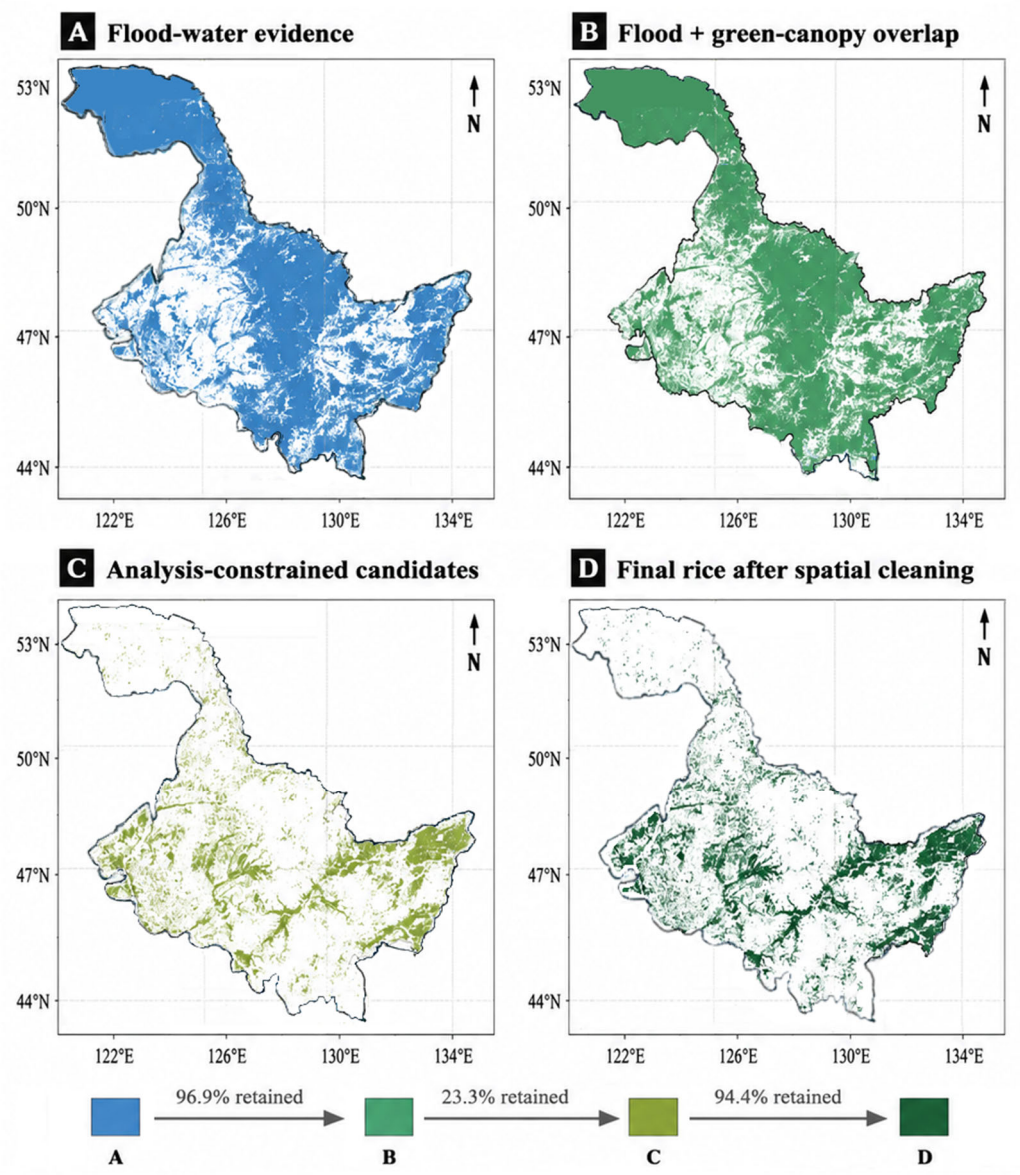


Figure 7. Sequential spatial screening of rice candidates within the 2025 analysis domain in Heilongjiang Province. (**A**) Early-season optical flood-water evidence, 33.00 Mha; (**B**) candidates satisfying both flood-water and subsequent green-canopy conditions, 31.99 Mha (96.9% of Stage (**A**));

(**C**) candidates satisfying the integrated phenological rule and analysis-mask constraints, 7.44 Mha (23.3% of Stage (**B**)); and (**D**) final mapped rice after connected-component filtering and neighbourhood-based spatial refinement, 7.02 Mha (94.4% of Stage (**C**)).

Table 5. Sequential reduction of rice-candidate area within the 2025 analysis domain.

Stage	Screening Condition	Area	Relative Area from Previous Stage (%)
A	Flood-water evidence	33.00 Mha	—
B	Flood water and green canopy	31.99 Mha	96.9%
C	Stage B restricted to the analysis domain and supporting phenology	7.44 Mha	23.3%
D	Final rice following spatial post-processing	7.02 Mha	94.4%

3.6. Component Sensitivity and Benchmark Comparison

Component sensitivity was evaluated by modifying individual evidence pathways, environmental constraints, and spatial post-processing settings while retaining all other parameters unchanged (Table 6). The "No SAR" configuration represents an optical-only phenological baseline in which rice candidates were supported by the optical flood-water, green-canopy, and green-rise conditions without Sentinel-1 flood support, whereas the "No green-rise" configuration retained SAR support but removed the optical greenness-transition pathway.

Table 6. Component sensitivity and ablation analysis of the rice-mapping framework.

Configuration	Area (Mha)	OA (%)	Rice PA (%)	Rice UA (%)	Rice F1 (%)
Full model	7.02	92.09	94.87	75.90	84.33
Optical-only support (No SAR)	6.60	92.37	89.22	80.98	84.90
No green-rise	5.95	93.24	87.36	83.06	85.15
No cropland mask	7.48	91.80	94.87	73.96	83.16
No water exclusion	7.56	91.37	94.87	74.00	83.15
No focal-mode	6.86	91.65	94.87	74.75	83.62
8-pixel minimum	6.89	92.52	92.50	77.08	84.09

The ablation results revealed a trade-off between rice-detection sensitivity and mapped-class precision (Table 6). Relative to the full framework, the optical-only configuration (No SAR) reduced mapped area from 7.02 to 6.60 Mha and decreased rice producer's accuracy from 94.87% to 89.22%, while increasing user's accuracy from 75.90% to 80.98%. Removing the optical green-rise pathway produced a smaller mapped area of 5.95 Mha and further reduced producer's accuracy to 87.36%, although user's accuracy increased to 83.06%. These results indicate that the combined SAR and optical support pathways primarily improve rice detection sensitivity, whereas individual pathways produce more conservative mapped areas. Separately, removing the cropland mask, water exclusion, or focal-mode refinement quantified the effects of environmental masking and spatial post-processing independently from the phenological evidence pathways.

For benchmark comparison, the proposed framework and a 200-tree Random Forest classifier were evaluated on the same held-out reference subset using identical seasonal optical and SAR variables (Table 7). The metrics in Table 7 were calculated only from this common test subset and therefore differ from the full-validation metrics reported in Table 6.

Table 7. Comparison of the proposed framework and Random Forest on the same held-out reference subset.

Method	OA (%)	Rice PA (%)	Rice UA (%)	Rice F1 (%)
Proposed framework	93.53	95.00	84.44	89.41
Random Forest	89.93	89.47	77.27	82.93

On the shared held-out subset, the proposed framework achieved higher performance than the Random Forest baseline across all reported metrics (Table 7). Overall accuracy increased from 89.93% to 93.53%, while rice producer's accuracy, user's accuracy, and F1-score increased from 89.47%, 77.27%, and 82.93% to 95.00%, 84.44%, and 89.41%, respectively. These results demonstrate that explicitly representing the flood-to-green phenological sequence provided improved discrimination relative to the conventional Random Forest baseline under the same evaluation conditions.

4. Discussion

4.1. Spatial Performance Within the Analytical Domain

The Sentinel-1/2 flood-to-green framework successfully captured the characteristic phenological trajectory of paddy rice, where early-season inundation is followed by rapid vegetation development. The spatial distribution of mapped rice was consistent with the agricultural characteristics of Heilongjiang Province, where rice cultivation is concentrated in low-lying plains with intensive irrigation and strong seasonal water-management practices. The results demonstrate that rice identification benefits from representing crop development as a temporal process rather than relying on individual spectral observations.

Previous rice-mapping studies have increasingly exploited multi-temporal optical and radar observations to improve classification performance. Sentinel-1 and Sentinel-2 integration has been shown to provide complementary information under cloud-prone conditions, while phenology-based approaches improve discrimination by incorporating crop growth characteristics [33]. Automated frameworks such as FARM and SPRC further demonstrated the potential of combining phenological features with machine-learning classifiers for large-area rice mapping [13,34]. However, many existing approaches still depend on training samples, feature selection procedures, or classifier optimization, which may limit reproducibility when applied to new regions or years.

A direct numerical comparison with published phenology-based frameworks was not attempted because those methods use different training strategies, feature sets, study periods, and validation designs. Their reported accuracies are therefore not directly comparable with the present experiment. Instead, the contribution of phenological evidence was evaluated internally through the optical-only and pathway-removal ablations in Table 6, while a conventional Random Forest baseline was evaluated on a common held-out subset in Table 7.

The major contribution of this study is the development of an interpretable evidence-based framework in which each rice pixel is supported by explicit phenological and environmental conditions. Rather than treating Sentinel-1 and Sentinel-2 observations as independent classification variables, the proposed method organizes them according to the physical sequence of rice growth: early water response, canopy development, and flood-to-green transition [35,36]. This design improves transparency and enables the contribution of individual evidence components to be evaluated. Such interpretability is increasingly important for operational remote sensing products where users require not only accurate maps but also information on the mechanisms supporting classification decisions [37].

4.2. Mapping Performance, Uncertainty, and Operational Applicability

The validation results indicate that the framework achieved reliable rice detection within the analyzed domain, with an overall accuracy of 92.09%, rice producer's accuracy of 94.87%, user's accuracy of 75.90%, and an F1-score of 84.33%. The high producer's accuracy suggests that the flood-to-green constraints effectively captured most reference rice locations. However, the lower user's accuracy indicates that commission errors remain the primary challenge, mainly due to confusion with other agricultural or wetland environments exhibiting similar combinations of moisture and vegetation responses. The false-positive analysis further showed that most commission errors occurred in other cropland, suggesting that non-rice crops exhibiting strong summer greenness and occasional early-season wetness can partially mimic the flood-to-green rice signal.

The rule-support analysis complements the independent accuracy assessment by distinguishing rice pixels supported by both SAR and optical phenological pathways from those supported by only one pathway. The 59.5% reduced-support proportion should therefore be interpreted as a measure of internal evidence consistency rather than as an error probability. Independent classification error is reported separately through the confusion-matrix-based accuracy assessment.

The framework also provides operational advantages because it does not require extensive manual training samples or repeated classifier optimization. The use of Sentinel-1/2 observations and Google Earth Engine provides a practical basis for future annual updating, while the rule-based structure facilitates interpretation. However, transferability requires additional validation across years and regions. However, the framework should be considered a phenology-based mapping approach rather than a complete province-wide rice inventory because validation and area interpretation are limited to the defined analytical domain. From an agricultural monitoring perspective, the proposed framework offers three practical advantages. First, the use of Sentinel-1/2 time-series observations enables repeatable monitoring without dependence on extensive field sampling. Second, the flood-to-green phenological representation corresponds to recognizable rice cultivation processes, improving interpretability for agricultural users. Third, the rule-based architecture facilitates annual updating by adjusting regional phenological windows rather than rebuilding complex classification models.

4.3. Limitations and Future Improvements

Several limitations should be considered. First, the framework was evaluated for a single growing season in Heilongjiang Province. Although the region provides an appropriate test environment because of its strong rice flooding and canopy-development signals, further evaluation across multiple years and different rice-producing regions is required to assess transferability.

Second, the current framework relies on predefined phenological periods and empirical thresholds. These parameters were selected according to regional rice-growth characteristics and exploratory separation of rice and non-rice responses but may require adjustment under different planting calendars, irrigation practices, climatic conditions, and Sentinel-1 acquisition geometries. In particular, the VV and VH flood thresholds may be sensitive to incidence-angle and orbit-related variations because no additional incidence-angle normalization was applied in the present implementation. Future studies could incorporate incidence-angle-aware normalization together with adaptive phenological detection, crop calendars, or temperature-based growth models to improve transferability. Future work should further evaluate temporal-window sensitivity across multiple years and regions to quantify the robustness of fixed seasonal periods.

Third, the classification is influenced by the static ESA WorldCover 2021 cropland layer used to define the agricultural analysis domain. The sensitivity experiment showed

that removing this constraint increased the mapped rice area from 7.02 to 7.48 Mha while slightly reducing overall accuracy, rice user's accuracy, and F1-score; rice producer's accuracy remained unchanged. This indicates that the cropland constraint primarily suppresses additional commission-prone detections outside the mapped agricultural domain. Nevertheless, because the WorldCover layer predates the 2025 study year, genuine land-cover changes between 2021 and 2025 may not be fully represented. Future applications could therefore incorporate more temporally current or dynamically derived cropland masks to reduce dependence on a static land-cover product. However, because the validation design did not provide a design-based sample of 2025 rice outside the WorldCover cropland domain, potential omissions caused by genuine cropland expansion or land-cover change outside the 2021 mask could not be directly quantified.

Additional information, including field boundaries, elevation, irrigation datasets, or dynamic cropland masks, could further improve discrimination.

Finally, the strength of the proposed framework is its transparency and simplicity, but this also introduces limitations compared with more complex machine-learning approaches. Future research could explore hybrid strategies that combine interpretable phenological rules with weakly supervised or uncertainty-aware learning models, maintaining physical interpretability while improving adaptability in heterogeneous agricultural landscapes.

5. Conclusions

This study developed an interpretable Sentinel-1/2 flood-to-green phenology framework for rice mapping within selected agricultural regions of Heilongjiang Province. The framework combined early-season optical water evidence, subsequent canopy development, Sentinel-1 flood support, cropland constraints, permanent-water exclusion, and spatial post-processing through explicit and auditable decision rules.

The classification achieved a sample-based overall accuracy of 92.09%, a kappa coefficient of 0.791, a rice producer's accuracy of 94.87%, a rice user's accuracy of 75.90%, and an F1-score of 84.33%. These results indicate strong detection of reference rice locations, although commission error remained the dominant source of disagreement.

Because the analytical domain did not include the complete provincial extent, the resulting map must not be presented as a province-wide rice inventory. Within the defined 2025 analysis domain, the final classification identified approximately 7.02 Mha of rice. The estimate was derived directly from the final binary classification using pixel-area weighting and refers to the effective mapping domain established by the cropland, water-exclusion, phenological, and valid-observation constraints. The present findings therefore concern the spatial distribution and classification performance of rice within the analyzed regions rather than the total rice area of Heilongjiang.

The principal contribution of the framework lies in its transparent integration of phenological, radar, optical, and environmental evidence. Future work should extend the analysis to the complete province, verify mapped area through pixel-area calculations, conduct probability-based area estimation, and evaluate the method across multiple seasons and agricultural regions.

Author Contributions: Conceptualization, M.N.A. and S.Y.; methodology, M.N.A.; validation, M.N.A.; formal analysis, M.N.A.; data curation, S.Y. and M.N.A.; writing—original draft preparation, M.N.A.; writing—review and editing, X.Y. and G.D.B.; visualization, M.N.A. and S.Y.; supervision, L.G.; funding acquisition, X.Y. All authors have read and agreed to the published version of the manuscript.

Funding: This research received no external funding.

Data Availability Statement: Sentinel-1 and Sentinel-2 imagery are publicly available through the Copernicus Data Space and Google Earth Engine platforms. ESA WorldCover and JRC Global Surface Water products are publicly accessible from their respective repositories. The derived rice classification maps, evidence layers, reference samples used for validation, and processing scripts will be made available through https://github.com/mnasarahmad/Rice_Mapping_Heilongjiang.git upon publication.

Acknowledgments: The authors acknowledge the European Space Agency (ESA) for providing Sentinel-1 and Sentinel-2 satellite data through the Copernicus Programme. We also thank the Google Earth Engine platform for providing cloud-based geospatial computing resources that enabled large-scale satellite data processing. The authors acknowledge the European Commission Joint Research Centre (JRC) for providing the Global Surface Water datasets and ESA WorldCover for providing global land-cover information used in this study. We also thank the organizations and researchers who contributed publicly available reference datasets that supported the validation analysis.

Conflicts of Interest: The authors declare no conflicts of interest.

References

1. Liang, Q.; Di, Y.; Hao, X.; Zhang, J.; Ci, M.; Sun, F.; Wang, C.; Fan, X.; Guo, X. A 30 m Multi-Year Dataset of Major Crop Distributions in Xinjiang, China (2013–2024) Based on Harmonized Landsat–Sentinel-2 Data. *Sci. Data* **2026**, *13*, 730. https://doi.org/10.1038/s41597-026-07082-w.
2. Fang, H.; Liang, S.; Chen, Y.; Ma, H.; Li, W.; He, T.; Tian, F.; Zhang, F. A Comprehensive Review of Rice Mapping from Satellite Data: Algorithms, Product Characteristics and Consistency Assessment. *Sci. Remote Sens.* **2024**, *10*, 100172. https://doi.org/10.1016/j.srs.2024.100172.
3. Xiao, D.; Niu, H.; Guo, F.; Zhao, S.; Fan, L. Monitoring Irrigation Dynamics in Paddy Fields Using Spatiotemporal Fusion of Sentinel-2 and MODIS. *Agric. Water Manag.* **2022**, *263*, 107409.
4. Yang, L.; Driscol, J.; Sarigai, S.; Wu, Q.; Lippitt, C.D.; Morgan, M. Towards Synoptic Water Monitoring Systems: A Review of AI Methods for Automating Water Body Detection and Water Quality Monitoring Using Remote Sensing. *Sensors* **2022**, *22*, 2416.
5. Li, X.; Yang, G.; He, M.; Xiong, Y.; Liu, L.; Mariam, H.; Ali, I.; Jiang, C.; Yao, X.; Zhu, Y.; et al. Automated Rice Mapping under Diverse Cropping Patterns and Establishment Methods by Integrating Phenological Knowledge and Synergy of Optical and SAR Imagery. *Remote Sens. Environ.* **2026**, *335*, 115255. https://doi.org/10.1016/j.rse.2026.115255.
6. Khachoo, Y.H.; Cutugno, M.; Robustelli, U.; Pugliano, G. Google Earth Engine Since 2022: A Structured Bibliometric Review of GeoAI-Driven Trends and Applications. *Sustainability* **2026**, *18*, 6241.
7. Chen, C.; Wang, L.; Yang, G.; Sun, W.; Song, Y. Mapping of Ecological Environment Based on Google Earth Engine Cloud Computing Platform and Landsat Long-Term Data: A Case Study of the Zhoushan Archipelago. *Remote Sens.* **2023**, *15*, 4072.
8. Ghosh, S.; Kumar, D.; Kumari, R. Cloud-Based Large-Scale Data Retrieval, Mapping, and Analysis for Land Monitoring Applications with Google Earth Engine (GEE). *Environ. Chall.* **2022**, *9*, 100605.
9. Shen, G.; Liao, J. Paddy Rice Mapping in Hainan Island Using Time-Series Sentinel-1 SAR Data and Deep Learning. *Remote Sens.* **2025**, *17*, 1033.
10. Mallet, P.; Béchet, A.; Galewski, T.; Mesleard, F.; Hilaire, S.; Lefebvre, G.; Poulin, B.; Sirami, C. Different Components of Landscape Complexity Are Necessary to Preserve Multiple Taxonomic Groups in Intensively-Managed Rice Paddy Landscapes. *Agric. Ecosyst. Environ.* **2022**, *328*, 107864.
11. Wei, J.; Cui, Y.; Luo, W.; Luo, Y. Mapping Paddy Rice Distribution and Cropping Intensity in China from 2014 to 2019 with Landsat Images, Effective Flood Signals, and Google Earth Engine. *Remote Sens.* **2022**, *14*, 759.
12. Ma, X.; Huang, Z.; Zhu, S.; Fang, W.; Wu, Y. Rice Planting Area Identification Based on Multi-Temporal Sentinel-1 SAR Images and an Attention U-Net Model. *Remote Sens.* **2022**, *14*, 4573.
13. Gao, Y.; Pan, Y.; Zhu, X.; Li, L.; Ren, S.; Zhao, C.; Zheng, X. FARM: A Fully Automated Rice Mapping Framework Combining Sentinel-1 SAR and Sentinel-2 Multi-Temporal Imagery. *Comput. Electron. Agric.* **2023**, *213*, 108262. https://doi.org/10.1016/j.compag.2023.108262.
14. Guo, X.; Bai, L. ACBE-CroFuseNet: An Optical and SAR Cross-Fusion Semantic Segmentation Network for Paddy Rice Extraction. *AI* **2026**, *7*, 302.

15. Wang, G.; Meng, D.; Chen, R.; Yang, G.; Wang, L.; Jin, H.; Ge, X.; Feng, H. Automatic Rice Early-Season Mapping Based on Simple Non-Iterative Clustering and Multi-Source Remote Sensing Images. Remote Sens. 2024, 16(2), 277. https://doi.org/10.3390/rs16020277.
16. Wang, Z.; Ma, Y.; Zhang, Y. Review of Pixel-Level Remote Sensing Image Fusion Based on Deep Learning. *Inf. Fusion* **2023**, *90*, 36–58.
17. Zhang, C.; Zhang, H.; Tian, S. Phenology-Assisted Supervised Paddy Rice Mapping with the Landsat Imagery on Google Earth Engine: Experiments in Heilongjiang Province of China from 1990 to 2020. *Comput. Electron. Agric.* **2023**, *212*, 108105. https://doi.org/10.1016/j.compag.2023.108105.
18. Heilongjiang Provincial Bureau of Statistics. *Heilongjiang Statistical Yearbook 2025*; Heilongjiang Provincial Bureau of Statistics: Harbin, China, 2025.
19. Qiu, J.; Shen, Z.; Xie, H. Drought Impacts on Hydrology and Water Quality under Climate Change. *Sci. Total Environ.* **2023**, *858*, 159854.
20. Gorelick, N.; Hancher, M.; Dixon, M.; Ilyushchenko, S.; Thau, D.; Moore, R. Google Earth Engine. *Remote Sens. Environ.* **2017**, *202*, 18–27.
21. Bian, L.; Li, B.; Wang, J.; Gao, Z. Multi-Branch Stacking Remote Sensing Image Target Detection Based on YOLOv5. *Egypt. J. Remote Sens. Sp. Sci.* **2023**, *26*, 999–1008.
22. Wang, J.; Li, X.; Zhao, M. EfficientFormer: Lightweight Convolution-Transformer Hybrid Model for UAV-Based Agriculture Mapping. *Comput. Electron. Agric.* **2024**, *210*, 108120.
23. Zanaga, D.; Van De Kerchove, R.; Daems, D.; De Keersmaecker, W.; Brockmann, C.; Kirches, G.; Wevers, J.; Cartus, O.; Santoro, M.; Fritz, S. ESA WorldCover 10 m 2021 V200. 2022. Available online: https://zenodo.org/records/7254221 (accessed on 13 December 2025).
24. Pekel, J.F.; Cottam, A.; Gorelick, N.; Belward, A.S. High-Resolution Mapping of Global Surface Water and Its Long-Term Changes. *Nature* **2016**, *540*, 418–422.
25. Li, H.; Pan, B.; Xu, R.; Liu, Z.; Pan, Y.; Zhang, X. Phenology-Guided Deep Learning for Automated Rice Mapping Using SAR Time-Series Imagery. *Int. J. Digit. Earth* **2026**, *19*, 2620881.
26. Wang, W.; Liu, S.; Yang, H.; Li, N.; Zhao, J.; Wu, W.; Zheng, W. A Phenology-Guided Multi-Source Framework for In-Season Rice Mapping in Cloud-Prone and Complex Agroecosystems. *Remote Sens.* **2026**, *18*, 1828.
27. Rouse, J.W.; Haas, R.H.; Schell, J.A.; Deering, D.W. Monitoring Vegetation Systems in the Great Plains with ERTS. In *Proceedings of the Third Earth Resources Technology Satellite-1 Symposium*; NASA: Washington, DC, USA, 1974; Volume 351, pp. 309–317.
28. Huete, A.; Didan, K.; Miura, T.; Rodriguez, E.P.; Gao, X.; Ferreira, L.G. Overview of the Radiometric and Biophysical Performance of the MODIS Vegetation Indices. *Remote Sens. Environ.* **2002**, *83*, 195–213. https://doi.org/10.1016/S0034-4257(02)00096-2.
29. Xiao, X.; Boles, S.; Frolking, S.; Li, C.; Babu, J.Y.; Salas, W.; Moore, B. Mapping Paddy Rice Agriculture in Southern China Using Multi-Temporal MODIS Images. *Remote Sens. Environ.* **2005**, *95*, 480–492. https://doi.org/10.1016/j.rse.2004.12.009.
30. Xu, H. Modification of Normalised Difference Water Index (NDWI) to Enhance Open Water Features in Remotely Sensed Imagery. *Int. J. Remote Sens.* **2006**, *27*, 3025–3033.
31. Yang, M.; Guo, B.; Wang, J. A Novel and Robust Method for Large-Scale Single-Season Rice Mapping Based on Phenology and Statistical Data. *ISPRS J. Photogramm. Remote Sens.* **2024**, *213*, 14–32. https://doi.org/10.1016/j.isprsjprs.2024.05.019.
32. Olofsson, P.; Foody, G.M.; Herold, M.; Stehman, S.V.; Woodcock, C.E.; Wulder, M.A. Good Practices for Estimating Area and Assessing Accuracy of Land Change. *Remote Sens. Environ.* **2014**, *148*, 42–57. https://doi.org/10.1016/j.rse.2014.02.015.
33. Cai, Y.; Guan, K.; Peng, J.; Wang, S.; Seifert, C.; Wardlow, B.; Li, Z. A High-Performance and in-Season Classification System of Field-Level Crop Types Using Time-Series Landsat Data and a Machine Learning Approach. *Remote Sens. Environ.* **2018**, *210*, 35–47.
34. Li, J.; Xue, F.; Li, G.; Zhang, M.; Tian, J.; Zhang, H. SPRC: A Novel Sentinel-1/-2 Phenology-Enhanced Framework for Automated Paddy Rice Mapping. *Int. J. Appl. Earth Obs. Geoinf.* **2025**, *143*, 104772. https://doi.org/10.1016/j.jag.2025.104772.
35. Phiri, D.; Simwanda, M.; Salekin, S.; Nyirenda, V.R.; Murayama, Y.; Ranagalage, M. Sentinel-2 Data for Land Cover/Use Mapping: A Review. *Remote Sens.* **2020**, *12*, 2291.
36. Lin, K.-F.; Perissin, D. Single-Polarized SAR Classification Based on a Multi-Temporal Image Stack. *Remote Sens.* **2018**, *10*, 1087.
37. Zhao, R.; Li, Y.; Ma, M. Mapping Paddy Rice with Satellite Remote Sensing: A Review. *Sustainability* **2021**, *13*, 503.

Disclaimer/Publisher's Note: The statements, opinions and data contained in all publications are solely those of the individual author(s) and contributor(s) and not of MDPI and/or the editor(s). MDPI and/or the editor(s) disclaim responsibility for any injury to people or property resulting from any ideas, methods, instructions or products referred to in the content.